

pubs.acs.org/IECR Article

Regenerable Sorbent Pellets for the Removal of Dilute H₂S from Claus Process Tail Gas

Wenyang Zhao, Michael Manno, Yasser Al Wahedi,* Michael Tsapatsis,* and Andreas Stein*



Cite This: Ind. Eng. Chem. Res. 2021, 60, 18443-18451



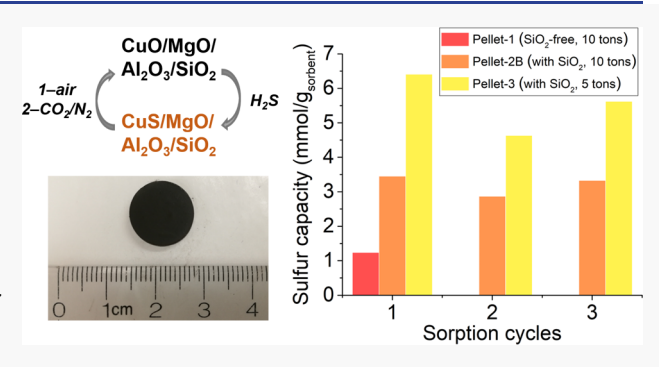
ACCESS I

Metrics & More

Article Recommendations

3 Supporting Information

ABSTRACT: The Claus process is the most important sour gas sweetening process to recover elemental sulfur from H₂S, which is present in raw natural gas and byproduct gases from crude oil refineries. However, current methods for treating the tail gas of the Claus process are expensive and often not environmentally friendly. Various sorbents have been reported for H₂S capture, but few reports focus on the pellet design, formation, and testing. In this study, we developed a pelletization method to prepare sorbent pellets with high sulfur capacity and good regenerability for the removal of dilute H₂S from Claus process tail gas. The sorbent pellets consisted of mixed metal oxides of Cu, Mg, and Al with fumed silica as the binder and were characterized using various techniques, including X-ray and



electron diffraction, N_2 sorption, and scanning and transmission electron microscopy. The H_2S sorption capacity was evaluated by breakthrough experiments at 150 °C in a gas stream consisting of 100 ppm of H_2S in N_2 . The optimized sorbent pellets gave a stable breakthrough sulfur capacity of \sim 5 mmol/g over three cycles of sulfidation and regeneration. They exhibited an average radial crush strength of 154 \pm 40 N.

1. INTRODUCTION

Hydrogen sulfide (H₂S) is commonly present in raw natural gas. If natural gas is harvested from a reservoir and used directly, H₂S will cause detrimental effects to natural gas liquefaction and storage facilities, such as corrosion of pipelines and deactivation of catalysts. 1,2 Natural gas processing starts at the well where raw natural gas is collected on the ground, and H₂S as well as other impurities, such as H₂O and CO₂, are removed.³ Acidic gases including H₂S and CO₂ are typically removed using polymeric membranes or amine treatments.^{4,5} Because of the economic value of sulfur, the mixture of H₂S and CO₂ is then collected and routed to the sulfur recovery unit. The Claus process is by far the most widely used process for sulfur recovery, in which H2S is converted to elemental sulfur and is later used in various applications, such as manufacturing of sulfuric acid, medicine, cosmetics, fertilizers, and rubber products.0

The catalytic reaction of oxidizing H_2S to sulfur is favored at low temperature and is carried out between 190 and 210 °C in the Claus furnace. However, due to the equilibrium of the conversion, the tail gas from the Claus process invariably contains a few ppmv to ~1000 ppmv of unreacted H_2S , which is above the permissible emission level of H_2S in the United States. When combusted, H_2S generates SO_2 and leads to acid rain, causing human health problems and damage to aquatic ecosystems.

Various processes have been established to remove this last portion of H₂S from the Claus process tail gas, including

regenerative solvent-based methods (such as SCOT using amines and LO-CAT II using an iron-chelated complex), non-regenerative solvent-based methods (DynaWave with NaOH solutions), and sorption-based methods (such as MOST with V/Ce/Mg₂Al₂O₅ and Z-sorb with ZnO). Compared to solvent-based processes, the use of solid sorbents has been demonstrated to simplify the operation and process engineering of sulfur recovery units while generating less waste. A case study using Cu-exchanged zeolite Y sorbent indicated that temperature-swing adsorption has the most economic outlook.

Solid sorbents such as metal oxides, $^{15-20}$ activated carbons, $^{21-23}$ zeolites, $^{24-26}$ and metal-organic frameworks 27,28 have been synthesized and tested for selective H_2S capture. Among them, metal oxides are better candidates, especially for industrial-scale desulfurization, because they can be prepared in large quantities. However, very little research has focused on the pelletization process for practical application of the materials. As an example of a metal-oxide-based sorbent, we have demonstrated that a mixed metal oxide

Received: September 15, 2021
Revised: November 9, 2021
Accepted: November 30, 2021
Published: December 13, 2021





(MMO) consisting of CuO, MgO, and Al₂O₃ shows high sulfur capacity (\sim 7.5 mmol/g) and stability on the laboratory-scale for capturing H₂S at 100 and 1435 ppm levels. Moreover, the proposed sorption—regeneration process of the sorbent is compatible with integration in the Claus process by redirecting SO₂ formed during regeneration back to the Claus furnace; it can, therefore, achieve both effective sulfur capture and recovery ($2H_2S + SO_2 \rightarrow 3S + 2H_2O$). The preparation of the MMO involves the coprecipitation of Cu, Mg, and Al nitrate solutions with Na₂CO₃ solution and a calcination step, which yields the final product as a fine powder that is highly porous due to textural porosity.

The as-prepared sorbent is a powder consisting of nanometer- and micrometer-sized particles, which take up large volumes of space and can easily become electrostatically charged. In order to use the sorbent on a bulk scale, such as in an adsorption tower or adsorption bed, one essential step is to prepare the sorbent material in pellet form. Otherwise, the powder is likely to be lost in the gas stream and may cause reactor clogging and overheating. Pellets have several advantages over powders. They have much greater mechanical strength than powders, making the pellets resistant to collapse. They are also easier to store and transport, reducing the cost of processing labor work and time and the maintenance cost of the operating plants. Therefore, pelletization is an important process for any downstream industrial application of the sorbent, and it requires the sorbent to be prepared in pellet form in such a way that it maintains its sorption properties and remains regenerable.

Here, we demonstrate an efficient approach of sorbent pelletization that can maintain a high sorption capacity for the pellets, and we examine the performance of the prepared pellets using a bench-scale setup with 100 ppm of H_2S (to conform to the safety regulations of the laboratory). Whereas direct pelletization of the MMO powder results in a significant loss of breakthrough capacity, incorporation of fumed silica as an additive overcomes this problem. Fumed silica proves to be a good binder and helps to improve the sulfur capacity and stability of the sorbent pellet. With uniform mixing of fumed silica binder and MMO powder, the sorbent pellet shows a stable sulfur capacity of \sim 5 mmol/g for three cycles. The regeneration conditions were optimized so that the activity of the sorbent pellet can be restored under economically viable conditions using a combination of air and CO_2/N_2 at 650 °C.

2. EXPERIMENTAL METHODS

2.1. Materials. The chemicals used in this study were obtained from the following sources: copper nitrate trihydrate (ACS reagent, \geqslant 99%), magnesium nitrate hexahydrate (ACS reagent, \geqslant 98%), and aluminum nitrate nonahydrate (ACS reagent, \geqslant 98%) from Sigma-Aldrich; sodium carbonate anhydrous (powder/certified ACS) from Fisher Chemical; untreated fumed silica (CAB-O-SIL M-5) from Cabot; quartz wool (fine, 4 μ m) from Acros Organics; air, N₂, He, CO₂, and 100 ppmv H₂S in N₂ from Matheson; and 5% O₂ in N₂ from Praxair. Deionized water purified to a minimum resistivity of 18.2 M Ω ·cm with a Milli-Q PLUS reagent-grade water system was used in all experiments.

2.2. Synthesis of the Solid Sorbent. The sorbent was synthesized from a mixed solution containing 120 mL of $Cu(NO_3)_2$, 60 mL of $Mg(NO_3)_2$, and 20 mL of $Al(NO_3)_3$, each of which had a concentration of 1.25 mol/L before mixing. A plastic syringe was loaded with 200 mL of the mixed

metal nitrate solution. A separate 2000 mL polypropylene bottle was filled with 400 mL of deionized water and heated using an oil bath at 70 °C under vigorous stirring. The mixed metal nitrate solution was added to the polypropylene bottle at a rate of 20 mL/min using a syringe infusion pump. The pH of the entire reaction mixture was maintained at 7 by manual in situ addition of 1.25 mol/L Na₂CO₃ solution. Upon complete addition of the mixed metal nitrate solution, the reaction temperature was increased to 80 °C and kept there for 1 h under continuous stirring to age the mixture. The resulting precipitate was filtered and washed several times with deionized water until the pH of the filtrate was 7. The filter cake was then transferred into a Petri dish, dried at 70 °C for 12 h, and then calcined at 500 °C for 5 h in air flowing at a rate of ~100 mL/min. Approximately 13 g of final product was obtained as a loosely packed powder.

2.3. Sorbent Pellet Formation. 2.3.1. Pellet Formation without Binder. The MMO powder obtained after calcination was transferred and ground to a fine powder using a mortar and pestle. Approximately 500 mg of the powder was then placed in a 13 mm die set and pressed using a hydraulic press at 10 tons. The obtained solid pellet had a round cylindrical shape with a thickness of \sim 1.08 mm and a density of \sim 3.50 g/cm³. The pellet was crushed and sieved to 40–80 mesh for the sorption test.

2.3.2. Pellet Formation with Binder. In one experimental setup, the MMO powder obtained after calcination was ground into a fine powder using a mortar and pestle and mixed with fumed silica with an 85:15 mass ratio (MMO/silica). The powder mixture was ball-milled for 10 min in order to obtain a uniform mixture. After that, approximately 300 mg of the mixture was compacted using a hydraulic press at 10 tons. The pellet prepared this way had a thickness of ~0.69 mm and a density of ~3.30 g/cm³. In another experimental setup, a mixture with a mass ratio of MMO to fumed silica equal to 85:15 was ball-milled for 60 min, and approximately ~600 mg of powder was used for preparing the sorbent pellet. The powder mixture was pressed at 5 tons and also yielded solid pellets. The bulk density of the pellet was ~ 3.08 g/cm³, and the thickness was ~1.47 mm. The obtained solid pellet was ground and sieved to 40-80 mesh for the sorption tests. The different methods of pellet formation are summarized in Table

Table 1. Preparation Methods and Compositions of Different Sorbent Pellets

	MMO (wt %)	fumed silica (wt %)	ball-milling time (min)	pressure (tons)
pellet 1	100	0	0	10
pellet 2	85	15	10	10
pellet 3	85	15	60	5

2.4. H₂S Sorption. The experimental setup for sulfidation–regeneration studies was constructed from stainless steel 316 tubing and connections from Swagelok. The amounts of sorbent and quartz diluent used in each experiment are summarized in Table 2. Pellet 2 was tested under two different conditions, labeled as pellet 2A and pellet 2B. Typically, the sieved sorbent particles (mesh 40–80) were sandwiched between quartz wool plugs in a U-shaped quartz tube with a 4 mm inner diameter. Sorbents were activated under a 40 mL/min N₂ flow at 300 °C for 12 h and then exposed to an H₂S

Table 2. H₂S Sorption Conditions for Different Samples

	sorbent mass (mg)	quartz diluent (mg)	100 ppmv H ₂ S/N ₂ flow rate (mL/min)	sorbent bed residence time (s)
MMO powder	5.0	100.0	40	0.15
pellet 1	200.0	0	10	0.71
pellet 2A	200.0	0	10	0.83
pellet 2B	200.0	0	40	0.21
pellet 3	150.0	50.0	10	0.75

stream (100 ppmv in N_2 , Matheson) at 150 °C and 1 atm. The sulfur species concentration at the reactor exit was monitored using a gas chromatograph (Agilent 7890A) equipped with an Agilent DB-1 column and a sulfur chemiluminescence detector (SCD). This setup allowed detection of both H_2S and SO_2 . Breakthrough capacity was determined at an exit H_2S concentration equal to 5% of the inlet concentration. For pellet 2B and pellet 3, the sulfidation and regeneration were carried out consecutively for three cycles, and the corresponding regeneration conditions are shown in Table 3. The regeneration conditions were modified each time in search of the optimum. The reactor was flushed with N_2 for at least 15 min between cycles as a safety precaution. The flow rates were calibrated using a soap film flowmeter.

2.5. Characterization. Powder X-ray diffraction (XRD) patterns of the materials were obtained using a PANalytical X'Pert Pro diffractometer outfitted with an X'Celerator detector and a Co anode (K α radiation, $\lambda = 1.789$ Å) operating at 45 kV and 40 mA. Scanning electron microscopy (SEM) was performed on a JEOL-6500 field emission scanning electron microscope with an accelerating voltage of 5.0 kV. All samples were coated with a 50 Å platinum film prior to SEM imaging. Nitrogen sorption experiments were performed on a Quantachrome Autosorb-iQ2 analyzer. All samples were degassed under a dynamic vacuum (~0.003 mTorr) at 120 °C for 12 h before analysis. Brunauer-Emmett-Teller (BET) surface areas were evaluated from the adsorption isotherms in the relative pressure range 0.05-0.35. Barrett-Joyner-Halenda (BJH) pore volumes were calculated using the adsorption branch of the isotherms. Thermogravimetric analysis (TGA) and differential scanning calorimetry (DSC) experiments were performed on a Netzsch STA 409 instrument. Samples were heated in air at a ramp rate of 5 °C/min. Transmission electron microscopy (TEM) images were obtained using a FEI Tecnai T12 transmission electron microscope with a LaB₆ filament at an accelerating voltage of 120 kV. TEM samples were prepared by dispersing the materials on a carbon-coated Cu grid. Single pellet crush

strength was measured following the ASTM D4179 protocol³⁰ using an Instron 5966 universal testing system with a 10 kN load cell and compression plates, at an increasing force rate of 4.4 N/s. Eighteen samples were tested for the calculation of the average crush strength and its uncertainty at the 95% confidence level. The end-point of the test was taken to be the first point at which the resistance decreased as the load continued to increase.

3. RESULTS AND DISCUSSION

3.1. Performance Evaluation of MMO Powder. The MMO powder consists of CuO, MgO, and Al_2O_3 with composition $Cu_{6.2}Mg_{0.21}AlO_{7.9}$ determined by elemental analysis, where CuO is the only crystalline phase in the sample as shown in the XRD pattern (Figure S1). The average grain size of CuO was calculated to be 14 nm on the basis of the XRD pattern (Table S1). CuO is the active species in the sorbent that can react with H_2S during sorption. Reaction 1 shows the typical reaction between CuO and H_2S at 150 °C with a stoichiometry of 1:1, which results in the formation of CuS. Theoretically, if all of the CuO in the MMO powder reacts with H_2S by this pathway, the sulfur capacity will be 11.2 mmol/g.

$$CuO + H_2S \rightleftharpoons CuS + H_2O \tag{1}$$

The long-term stability of MMO powder was studied via multiple sorption-regeneration cycles. Once a H_2S sorption step was completed, desorption was carried out at 600 °C for 6 h with 5% O_2/N_2 , during which CuS was oxidized to CuSO₄, CuO·CuSO₄, and CuO after all the sulfur species had been desorbed. Reaction 2 shows the simplified overall reaction.

$$CuS + 1.5O_2 \rightleftharpoons CuO + SO_2 \tag{2}$$

Figure 1 shows the sulfur capacity of the MMO powder for 10 cycles, which stabilized at \sim 7.5 mmol/g, corresponding to a reaction efficiency of 67%. This indicates that the CuO in the MMO powder is highly reactive during cycling, even though its grain size has increased from 14 to 93 nm after the first regeneration (Figure S1 and Table S1).

3.2. Structural Characterization of Pellet 1 and Pellet 2A and Their H₂S Sorption Performance. High pressure was applied when preparing pellet 1 and pellet 2, where for pellet 1, only the MMO powder was pressed at 10 tons to obtain a self-sustaining pellet, whereas for pellet 2, fumed silica was added as the binder before pressing the pellet. As shown in Figure S2, the nitrogen sorption isotherm of MMO indicates that it contains mainly mesopores and macropores with a BET surface area of 52 m²/g. The isotherm has a type H3 hysteresis loop, which can usually be found in nonrigid aggregates of

Table 3. Regeneration Conditions for Sorbent Pellets at Different Stages

		first regeneration	second regeneration	third regeneration
pellet 2B (sorbent weight: 200 mg)	temperature	25-600 °C, 5 °C/min, hold at 600 °C	25-600 °C, 5 °C/min, hold at 600 °C	25–650 °C, 5 °C/min, hold at 650 °C
	stage 1	5% O ₂ /N ₂ , 100 mL/min, ~17.5 h	5% O ₂ /N ₂ , 100 mL/min, ~16.5 h	5% O ₂ /N ₂ , 100 mL/min, ~14 h
	stage 2	He, 40 mL/min, ~47.5 h	He, 40 mL/min, ~46 h	He, 40 mL/min, ~24 h
pellet 3 (sorbent weight: 150 mg, quartz diluent: 50 mg)	temperature	25-650 °C, 5 °C/min, hold at 650 °C	25-650 °C, 5 °C/min, hold at 650 °C	25–650 °C, 5 °C/min, hold at 650 °C
	stage 1	5% O ₂ /N ₂ , 100 mL/min, ~14 h	air, 100 mL/min, ~8 h	air, 100 mL/min, ~8 h
	stage 2	N_2 , 40 mL/min, ~31 h	$CO_2/N_2 = 1:1, 40 \text{ mL/min},$ ~24 h	CO_2/N_2 = 1:1, with ~6000 ppmv $H_2O(g)$, 40 mL/min, ~32 h

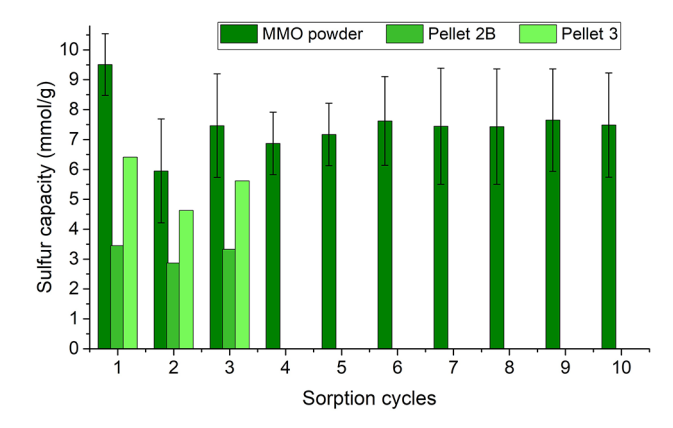


Figure 1. Summary of the sulfur sorption capacity of the MMO powder, pellet 2B, and pellet 3 over multiple cycles.

plate-like particles, corresponding well with the morphology of the MMO particles (Figure S3). After the high-pressure treatment at 10 tons, particles in the pellets are in closer contact with each other compared to the MMO powder, leading to a decrease of the macropores, as indicated by the decrease of the isotherm steps between the $\sim 0.9-1.0$ relative pressure range, which is representative of the macropores (Figure S2). At the same time, more mesopores appear as a result of compression, as shown in the hysteresis of type IV isotherms of pellet 1 and pellet 2 within the $\sim 0.35-0.95$ relative pressure range, as well as the change in mesopore volume percentage compared to the original MMO powder (Table S2).

In order to carry out the performance evaluation in a miniaturized fixed bed reactor, the round pellets were crushed and sieved to 40–80 mesh (Figure 2a and 2c), after which sieved particles stayed intact without obvious cracks on the exterior. According to the higher magnification SEM images in Figure 2b and d, no significant differences were found between pellet 1 (no silica) and pellet 2 (silica added) in terms of the surface textural details and morphologies. This indicates that the added fumed silica in the latter sample was uniformly mixed with the MMO powder.

Even though pellet 1 contained 100% MMO prepared from the MMO powder with a theoretical sulfur capacity of 11.2 mmol/g, the breakthrough capacity was calculated to be only 1.2 mmol/g from the breakthrough curve in Figure S4. With a total capacity of 1.4 mmol/g, the reaction efficiency of pellet 1 was only 12.3%. The breakthrough curve leveled out at the end, indicating that the reaction between CuO and $\rm H_2S$ had stopped, and thus the majority of the pellet was inactive. Compared to the MMO powder, which had a stable sulfur capacity of \sim 7.5 mmol/g for 10 cycles, the utilization of pellet 1 was much lower even for the fresh material.

The reaction between CuO and H_2S belongs to the category of noncatalytic gas—solid reactions. Hoffman et al. proposed that for the reaction between H_2S and metal oxides, H_2S first adsorbs at exposed metal centers at the surface of a metal oxide, forming a thin layer of metal sulfide, followed by diffusion of S^{2-} through the metal sulfide layers.³¹ The unit cell of CuS (a = 3.792 Å, c = 16.344 Å, V = 203.53 Å³, hexagonal, Z = 6 formula units (f.u.), $\rho = 4.68$ g/cm³) is much larger than that of CuO (a = 4.653 Å, b = 3.425 Å, c = 5.129 Å, V = 80.63 Å³, monoclinic, E = 4 f.u., E = 6.55 g/cm³), which corresponds to a volume expansion of 68%. The inevitable volume change leads to the increased mass transfer resistance in the dense pellet that prevented further reactions between CuO and E = 4.65

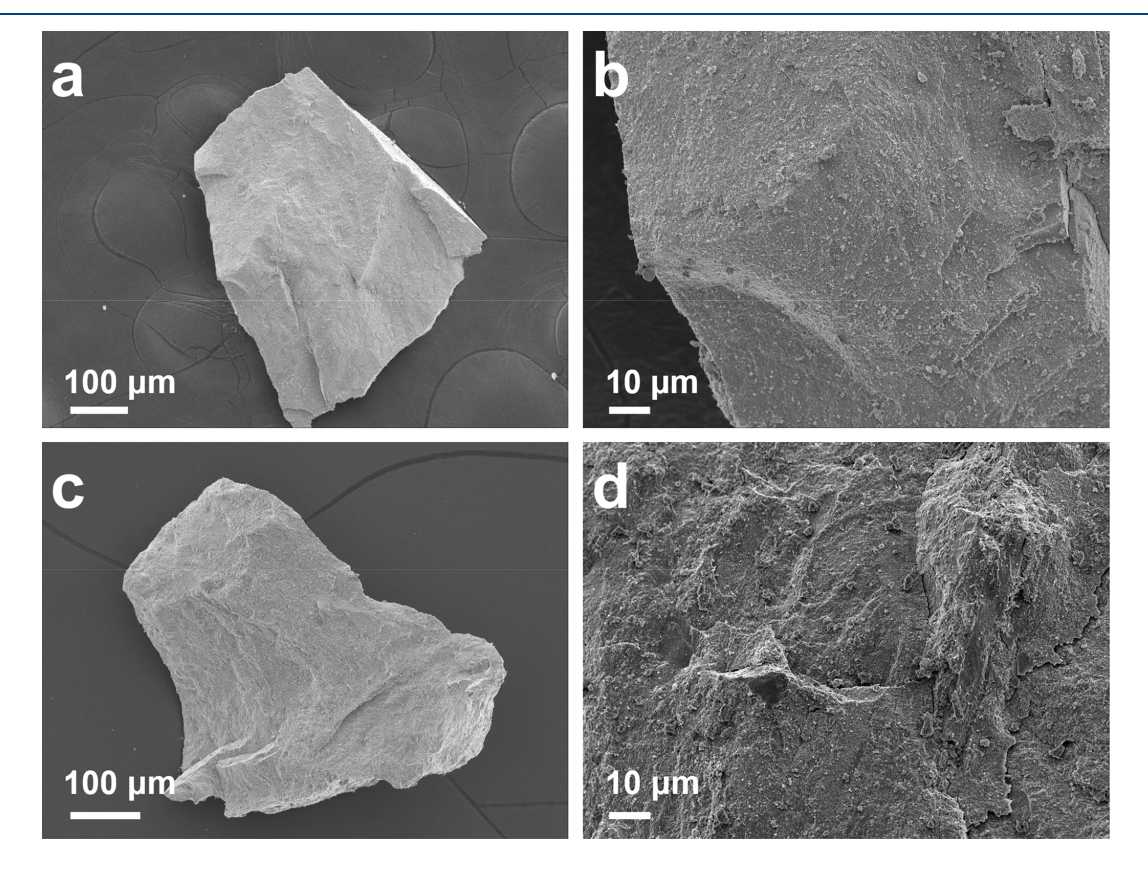


Figure 2. SEM images of the sieved sorbent pellet 1 (without silica, a and b) and pellet 2 (with added silica, c and d).

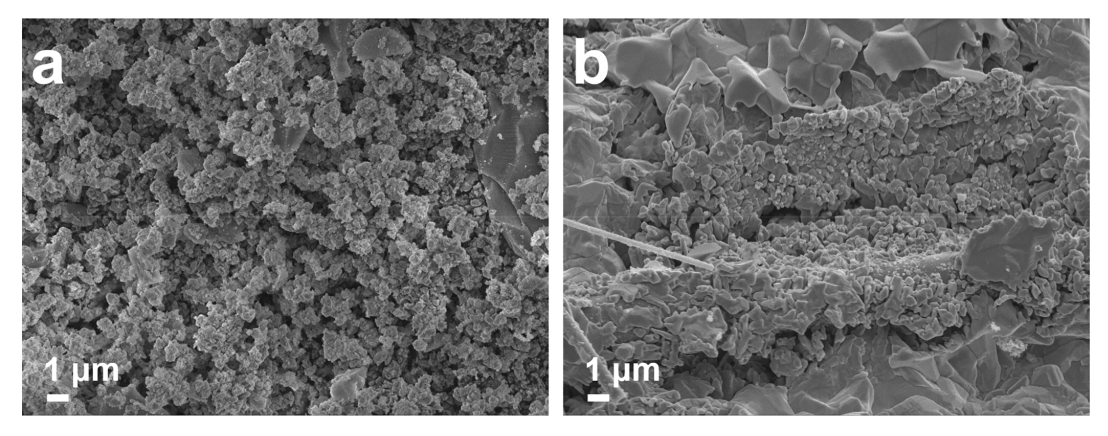


Figure 3. SEM images of the MMO powder after regeneration for 6 h at 600 °C (a) and pellet 2A after regeneration for 48 h at 600 °C (b).

To address these limitations, pellet 2A contained a mixture of MMO and fumed silica with a mass ratio of 85:15. The surface area of pellet 2A was 77 m²/g, which was higher than that of pellet 1 because of the added fumed silica with a high specific surface area (200 m²/g). The fumed silica works very well as a binder to maintain the shape of the pellet (Figure S5), and it also stabilizes the fragments obtained from pelletized particles after grinding and sieving (Figure 2c). The content of active material was less than in the undiluted material, and therefore, the theoretical capacity of the mixed metal oxide/ silica pellet was slightly lower (9.5 mmol/g). Nonetheless, as shown in Figure S6, the breakthrough capacity of pellet 2A was 7.6 mmol/g, with a reaction efficiency of 80%. This clearly indicates that fumed silica helps with the reaction between CuO and H2S and facilitates the diffusion of H2S into the pellet particles. According to the XRD pattern of pellet 2A, after the first sulfidation step (Figure S7), CuS was the dominant phase with some minor Cu₂S contribution, which suggests that all of the CuO in the sorbent had been consumed, leading to a high utilization of pellet 2A. The average grain size of CuS in pellet 2A after sulfidation, estimated from the XRD pattern, was 61 nm, close to that of the MMO powder (65 nm). This indicates that CuO in pellet 2A and in MMO powder behaved in a similar way during sulfidation (Figure S7 and Table S3). We hypothesize that the branched and chain-like fumed silica acts as a spacer that isolates MMO particles during pressing, promoting H₂S diffusion, and allowing the expansion from CuO to CuS during H₂S sorption, thus leading to a high reaction efficiency that is comparable to the MMO powder.

3.3. Regeneration of MMO Powder and Pellet 2A. During sulfidation, CuO in the sorbent reacts with H₂S and is converted to CuS. In order to reuse the sorbent, oxidation is required to convert CuS back to CuO. A study of the thermodynamics of the Cu–O–S system indicated that there is no direct conversion from CuS to CuO during oxidation, and several intermediates, including CuSO₄ and CuO·CuSO₄, appear before the material is fully converted to CuO.³² Another study focusing on the thermal oxidation of bulk CuS in air showed that at least 653 °C is needed to fully convert CuS to CuO.³³

We carried out the regeneration of MMO powder at $600\,^{\circ}\text{C}$ using $5\%\,O_2/N_2$ for 6 h, and the XRD data showed that all the sulfur-containing species had been converted under these conditions (Figure S1), leaving only CuO with a grain size of 93 nm (Table S1). However, the oxidation of CuS in pellet 2A

was much slower. As shown in Figure S8, after 6 h at 600 °C, the sample consisted of a mixture of CuO, CuO·CuSO₄, and CuSO₄. This different composition compared to the MMO powder was caused by the increased mass transfer resistance that had slowed down the process for O₂ to diffuse into the pellet and SO₃, a decomposition product of CuO·CuSO₄, to diffuse out. The regeneration time was prolonged to 48 h, after which some impurity peaks, possibly from CuO·CuSO₄, at \sim 28° 2 θ could still be observed in the XRD pattern (Figure S8).

Prolonged heat treatment is not desirable as it causes more sintering of the pellet compared to the MMO powder, not to mention that particles are already in close vicinity in the pellet, which further promotes the sintering process. In the MMO powder after regeneration, most particles have sizes of $\sim 1~\mu m$; in contrast, due to the sintering and prolonged heating, large particles with size $\sim 5~\mu m$ can be seen in the SEM image of pellet 2A (Figure 3). These large particles not only make it more difficult to fully regenerate the sorbent but also further slow down the reaction between CuO and H_2S during the next cycle. In fact, as shown in Figure S9, more than 5% SO₂ was detected during the second sulfidation of pellet 2A, suggesting that the sample was not fully regenerated, as CuO·CuSO₄ oxidized H_2S to SO₂, leading to a low reaction efficiency.

3.4. Stability of Pellet 2B over Three Cycles. With a residence time of 0.83 s of the sorption bed for pellet 2, it took over a month to finish a single cycle. In order to study the performance of the pellet over multiple cycles, we increased the flow rate of H₂S/N₂ from 10 mL/min to 40 mL/min while testing pellet 2 (labeled as pellet 2B), focusing on capacity changes over multiple cycles. Figure 4 shows the breakthrough curves of pellet 2B for three cycles, where the sulfur capacity stabilized at \sim 3.3 mmol/g. Only a negligible amount of SO₂ was formed during sorption, which would not affect the practical use of the sorbent pellet. As summarized in Table S4, the reaction efficiency of pellet 2B in the first cycle was lower compared to the sorption carried out with a slower H₂S flow rate, which was due to the shorter residence time that led to the earlier breakthrough of the sorption bed. However, the performance over three cycles indicates that pellet 2 can yield a stable sulfur capacity under appropriate regeneration con-

The regeneration conditions were further studied while monitoring the SO_2 concentrations in the effluent for pellet 2B. For the first regeneration, the temperature was increased from 25 to 600 °C with a heating rate of 5 °C/min. As shown in

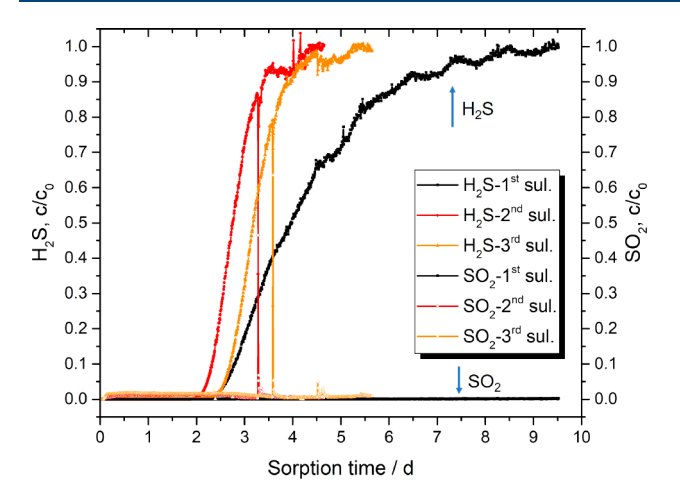


Figure 4. Breakthrough curve for pellet 2B. The sulfidation conditions were as follows: sorbent weight, 200 mg; sulfidation temperature, 150 $^{\circ}$ C; gas, 100 ppmv H₂S in N₂; flow rate, 40 mL/min. The regeneration conditions are summarized in Table 3.

Figure S10, a high concentration of SO₂ was detected during the first 2 h before the temperature reached 600 °C, which was likely due to reaction 3 and reaction 4 shown below.³² After the temperature reached 600 °C, the SO₂ concentration became steady but slowly decreased, because of the slow decomposition of CuO·CuSO₄ (reaction 5) and the equilibrium reaction 6.32 After ~15 h, the gas stream was switched to He, at which time a sudden increase in the SO₂ concentration was seen (Figure S10). On the basis of this observation, it is clear that after changing the gas stream to He, the O₂-free atmosphere shifted reaction 6 to the right and facilitated the decomposition of CuO·CuSO₄, leading to the spike of SO₂ shown in Figure S10. Therefore, for the practical regeneration of the pellet, a two-stage regeneration using an O₂ atmosphere followed by an O₂-free atmosphere is better than simply using O₂-containing gas streams.

$$2CuS + O_2 \rightleftharpoons Cu_2S + SO_2 \tag{3}$$

$$Cu_2S + 1.5O_2 \rightleftharpoons Cu_2O + SO_2 \tag{4}$$

$$CuO \cdot CuSO_4 \rightleftharpoons 2CuO + SO_3$$
 (5)

$$2SO_3 \rightleftharpoons 2SO_2 + O_2 \tag{6}$$

The regeneration was carried out at 650 $^{\circ}$ C during the third cycle. As shown in Figure S10, the overall time needed for the third regeneration was much shorter compared to the previous two regenerations performed at 600 $^{\circ}$ C. The SO₂ level reached 1 ppm after \sim 32 h, which indicated that the temperature was an important factor that dominates the regeneration process. By increasing the regeneration temperature, the overall regeneration time was shortened to \sim 1 day.

After three complete sulfidation—regeneration cycles, the packed sorbent bed was removed from the furnace for analysis. As shown in Figure S11b, the upper part of the sorbent bed was similar in appearance to that of the fresh one, with the typical black appearance from CuO. A comparison of SEM images of pellet particles before sorption (Figure 2c,d) and after one or three sorption—regeneration cycles (Figure S14) shows that particles remained similar in size and surface texture during these processes. Although some grain growth is seen at higher magnification, only a few cracks are formed on the surface. However, the lower part of the sorbent bed turned red

after three cycles. XRD confirmed the presence of Cu₂O in the lower part of the bed, which produced this red color (Figure S12). The phase stability diagram of the Cu-S-O system suggests that at 650 °C and at relatively low O2 partial pressure, Cu₂O forms preferentially over CuO (Figure S13), which is likely the reason for the formation of Cu₂O at the lower end of the sorbent bed that corresponds to the front of the regeneration stream. Cu₂O possibly formed during the He purge of regeneration, which leads to the conclusion that even though O₂ is not necessary during the decomposition of CuO· CuSO₄ (reaction 5), some amount of O₂ must be present to guarantee that CuO is not being reduced to Cu2O. Cu2O has a lower sulfur capacity than CuO, and its formation has a detrimental effect on the sorption capacity. However, in practice, this issue can be avoided by dosing He with O2 to maintain an O₂ level above 10 ppm in the regeneration stream.

3.5. Stability of Pellet 3 over Three Cycles. We developed another way of forming pellets that required less pressure. For pellet 3, the mixture of MMO and fumed silica was ball-milled for 1 h before compressing at 5 tons. As shown in Figure S15a, the resulting pellet remained self-supporting. The average radial crush strength of pellet 3 was measured to be $154 \pm 40 \, \text{N}$ (95% confidence interval, Figure S16), comparable to some other values reported in the literature (Table S5). The N_2 sorption isotherm indicated that pellet 3 contained mainly macropores, with much less N_2 uptake compared to pellet 1 and pellet 2, possibly because the long ball-milling time had already made the powder mixture very dense before pressing the pellet, thus leading to a low BET surface area and lower BJH total pore volume (Table S2).

The H_2S sorption was carried out with a slow flow rate of 10 mL/min, and the residence time of the sorbent bed was ~ 0.75 s. The breakthrough curves for the three cycles shown in Figure 5 indicated that pellet 3 had a stable sulfur capacity

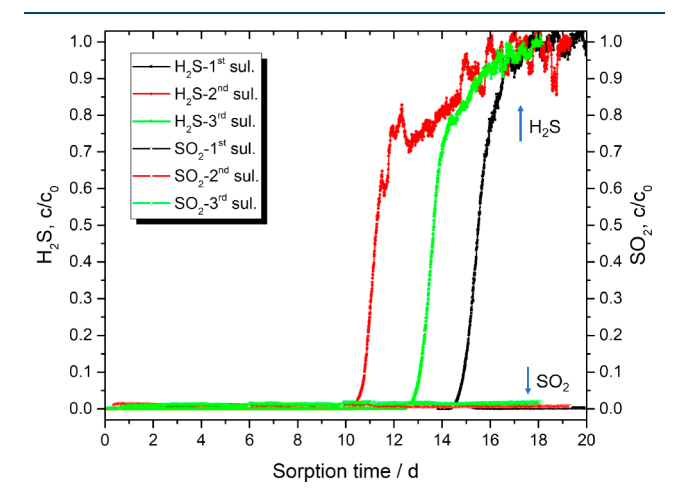


Figure 5. Breakthrough curves for pellet 3. The sulfidation conditions were as follows: sorbent weight, 150 mg; quartz diluent, 50 mg; sulfidation temperature, 150 $^{\circ}$ C; gas, 100 ppmv H₂S in N₂; flow rate, 10 mL/min. The regeneration conditions are summarized in Table 3.

using the regeneration conditions summarized in Table 2. The reaction efficiency of the first cycle was 70.5%, comparable to that of pellet 2A. This demonstrates that both approaches for preparing the sorbent pellets yield satisfactory outcomes with high reactivities and stable sulfur capacities (Table S6).

Because a high temperature can promote the overall regeneration process, for pellet 3, all three regenerations

were carried out at 650 °C. The first regeneration was performed at 650 °C with 5% $\rm O_2/N_2$ for 14 h before switching the gas stream to $\rm N_2$. As shown in Figure S17, a sudden increase of $\rm SO_2$ concentration was observed when changing the gas to $\rm N_2$. The $\rm SO_2$ behavior was similar to the regeneration of pellet 2B when switching from 5% $\rm O_2/N_2$ to He. This result further confirmed that an $\rm O_2$ -free environment is essential for the full decomposition of $\rm CuO\cdot CuSO_4$. As $\rm N_2$ is more economical and more abundant than He, the combination of $\rm O_2$ and $\rm N_2$ can further lower the total cost of regeneration.

In order to develop a more economical regeneration process, we proposed to use air during the initial stage of regeneration, and we also explored the possibility of carrying out the second stage of regeneration with CO2/N2. The tail gas of the Claus process usually contains H₂S ranging from a few ppmv to 0.1% and other gaseous components, such as CO₂ (20%); CO (1-2%); water vapor (20-25%); inert gases such as N_2 (50-60%); and ppmv levels of Ar, O2, H2, and hydrocarbons such as methane and ethane. Thus, the tail gas can possibly be used as the gas stream for regeneration with abundant N2 after H2S has been removed. Therefore, after the second sulfidation, which gave a reaction efficiency of 54.7%, we studied the second regeneration with air and CO₂/N₂. As shown in Figure S17, when air was used during the first 8 h and the gas stream was then changed to CO₂/N₂, the second regeneration was finished in ~32 h. In fact, the third sulfidation gave a satisfactory breakthrough capacity of 5.6 mmol/g (Table S6), suggesting that air and CO2/N2 are certainly suitable combinations for practical regeneration of the sorbent pellet.

During the third regeneration, H2O vapor was added to the regeneration stream of CO₂/N₂ with the aid of a gas bubbler. As shown in Figure S17, the concentration of SO₂ reached zero after ~22 h, which was much faster than in the case of the first and the second regeneration steps. We hypothesized that SO₃ and SO₂ reacted with H₂O from the stream (reaction 7 and reaction 8) and then cooled down and condensed as liquid H₂SO₄ and H₂SO₃ after leaving the hot zone of the reactor. Liquid H₂SO₄ and H₂SO₃ remained inside the tubing, so that SO₂ was no longer detected, but this cannot be used as an indication that the regeneration had finished. However, this issue can be addressed in a practical way by keeping the entire reactor at 650 °C during regeneration, as H₂SO₄ decomposes at 340 °C and reaction 7 and reaction 8 are only favored at a low temperature. The regeneration was continued for ~40 h. On the basis of the XRD data, all sulfate phases had decomposed after regeneration (Figure S1).

$$SO_3 + H_2O \rightleftharpoons H_2SO_4 \tag{7}$$

$$SO_2 + H_2O \rightleftharpoons H_2SO_3 \tag{8}$$

A new sorbent bed was prepared following the same conditions as for the previously used sorbent bed. As shown in Figure S18, the fresh cycle gave a reasonable sulfur capacity of 5.1 mmol/g, demonstrating the reproducibility of the sorption performance. Regenerations were carried out with air for 8 h and then changed to $O_2/N_2/H_2O(g)$ for 14 h at 650 °C. From Figure S18, the breakthrough capacities of the second and the third cycles were 2.7 mmol/g and 3.5 mmol/g, respectively. SO_2 detected in the effluent during regenerations showed a pattern similar to that of the first run of pellet 3 (Figure S19), where three different regeneration conditions were applied. It appears that when water vapor was added into the regeneration stream, the sulfur capacities were not as high as with the dry

regeneration stream. However, considering the additional step needed to remove the water vapor, the combination of air and $\rm CO_2/N_2/H_2O(g)$ can be a suitable alternative for regenerating the sorbent pellet.

4. CONCLUSIONS

We developed a pelletization method to prepare sorbent pellets from a MMO powder with high sulfur capacity and good regenerability for the removal of dilute concentrations of H_2S . With the addition of fumed silica as the binder, the prepared sorbent pellet shows a stable sulfur capacity of \sim 5 mmol/g under 100 ppmv H_2S in N_2 for three successive sorption—regeneration cycles at 150 °C. After the pellet was sulfidated, it could be regenerated by an economic method with a combination of air and CO_2/N_2 at 650 °C in \sim 1 day.

For the pelletization procedure, we discovered that fumed silica is an important component that helps to increase the reaction efficiency of the sorbent pellet. At the same time, it slows down the sintering of the pellet while maintaining its sulfur capacity. These findings provide practical guidelines for the preparation of similar sorbent pellets with complex compositions.

ASSOCIATED CONTENT

Supporting Information

The Supporting Information is available free of charge at https://pubs.acs.org/doi/10.1021/acs.iecr.1c03738.

XRD patterns, N_2 sorption isotherms, textural data, sample images, breakthrough curves, phase stability diagram (PDF)

AUTHOR INFORMATION

Corresponding Authors

Yasser Al Wahedi — Department of Chemical Engineering, Khalifa University of Science and Technology, Abu Dhabi, United Arab Emirates; Center for Catalysis and Separations, Khalifa University, Abu Dhabi, United Arab Emirates; Email: yasser.alwahedi@ku.ac.ae

Michael Tsapatsis — Department of Chemical Engineering and Materials Science, University of Minnesota, Minneapolis, Minnesota SS4SS, United States; Department of Chemical and Biomolecular Engineering and Institute for NanoBioTechnology, Johns Hopkins University, Baltimore, Maryland 21218, United States; Applied Physics Laboratory, Johns Hopkins University, Laurel, Maryland 20723, United States; occid.org/0000-0001-5610-3525; Email: tsapatsis@jhu.edu

Andreas Stein — Department of Chemistry, University of Minnesota, Minneapolis, Minnesota 55455-0431, United States; orcid.org/0000-0001-8576-0727; Email: astein@umn.edu

Authors

Wenyang Zhao – Department of Chemistry, University of Minnesota, Minneapolis, Minnesota 55455-0431, United States; orcid.org/0000-0002-0828-3813

Michael Manno – Department of Chemical Engineering and Materials Science, University of Minnesota, Minneapolis, Minnesota 55455, United States

Complete contact information is available at: https://pubs.acs.org/10.1021/acs.iecr.1c03738

Author Contributions

A.S., M.T., and Y.A.W. conceived the project and designed the experiments. W.Z. was responsible for the material synthesis, data collection, and analysis. M.M. and W.Z. were responsible for the mechanical test of the materials. A.S., M.T., Y.A.W., and W.Z. wrote the manuscript. All of the authors contributed to the discussion and preparation of the manuscript and the Supporting Information.

Notes

The authors declare no competing financial interest.

ACKNOWLEDGMENTS

This project was financially supported by the Gas Sub-Committee R&D arm of Abu Dhabi National Oil Company, United Arab Emirates. Y.A.W. acknowledges financial support from a Khalifa University of Science and Technology Center for Catalysis and Separations grant under RCII-2018-024. Parts of this work were carried out in the Characterization Facility, University of Minnesota, which receives partial support from the NSF through the MRSEC (Award Number DMR-2011401) and the NNCI (Award Number ECCS-2025124) programs. The authors would like to thank Professor R. Lee Penn for use of the powder X-ray diffractometer.

REFERENCES

- (1) Choi, Y.-S.; Nesic, S.; Ling, S. Effect of H_2S on the CO_2 corrosion of carbon steel in acidic solutions. *Electrochim. Acta* **2011**, 56, 1752–1760.
- (2) Shah, M. S.; Tsapatsis, M.; Siepmann, J. I. Hydrogen sulfide capture: From absorption in polar liquids to oxide, zeolite, and metalorganic framework adsorbents and membranes. *Chem. Rev.* **2017**, *117*, 9755–9803.
- (3) Kohl, A. L.; Nielsen, R. Gas Purification; Elsevier, 1997.
- (4) Miller, L. N.; Macriss, R. A.; Zawacki, T. S. Process for acid gas removal from gaseous mixtures. U.S. Patent US4,080,424, 1978.
- (5) Baker, R. W. Future directions of membrane gas separation technology. *Ind. Eng. Chem. Res.* **2002**, *41*, 1393–1411.
- (6) PiéPlu, A.; Saur, O.; Lavalley, J.-C.; Legendre, O.; Nédez, C. Claus catalysis and H₂S selective oxidation. *Catal. Rev.: Sci. Eng.* **1998**, 40, 409–450.
- (7) Kumar, P.; Sung, C.-Y.; Muraza, O.; Cococcioni, M.; Al Hashimi, S.; McCormick, A.; Tsapatsis, M. H₂S adsorption by Ag and Cu ion exchanged faujasites. *Microporous Mesoporous Mater.* **2011**, *146*, 127–133
- (8) Code of Federal Regulations. Title 40, Chapter I, Subchapter C, Part 60, Subpart J, §60.104 . Standards for sulfur oxides. Last revised September 2021. https://www.ecfr.gov/current/title-40/chapter-I/subchapter-C/part-60/subpart-J/section-60.104 (accessed September 14, 2021).
- (9) Eow, J. S. Recovery of sulfur from sour acid gas: A review of the technology. *Environ. Prog.* **2002**, *21*, 143–162.
- (10) DuPont, MECS DynaWave reverse jet scrubber technology. Reliable scrubbing of sulphur tank vents. *Sulphur*, **2011**, 336. https://cleantechnologies.dupont.com/fileadmin/user_upload/Editor/CleanTechnologies/documents/PDFs/55-Article_2011-Sulphur-Magazine-Reliable-scrubbing-of_sulphur_tank_vents.pdf (accessed September 14, 2021).
- (11) Buchanan, J. S.; Stern, D. L.; Nariman, K. E.; Teitman, G. J.; Sodomin, J. F.; Johnson, D. L. Regenerable solid sorbents for Claus tailgas cleanup: A treatment process for the catalytic removal of SO₂ and H₂S. *Ind. Eng. Chem. Res.* **1996**, 35, 2495–2499.
- (12) Strickland, J. F. Use of Z-Sorb process as catalytic incinerator for tail gas from sulfur plants. U.S. Patent US5,780,000, 1998.
- (13) McCabe, W. L.; Smith, J. C.; Harriott, P. *Unit Operations of Chemical Engineering*, 5th ed.; Operations Involving Particulate Solids, Vol. 5; McGraw-Hill: New York, 1993.

- (14) Al Wahedi, Y.; Torres, A. I.; Al Hashimi, S.; Dowling, N. I.; Daoutidis, P.; Tsapatsis, M. Economic assessment of temperature swing adsorption systems as Claus tail gas clean up units. *Chem. Eng. Sci.* 2015, 126, 186–195.
- (15) Xue, M.; Chitrakar, R.; Sakane, K.; Ooi, K. Screening of adsorbents for removal of H_2S at room temperature. *Green Chem.* **2003**, 5, 529–534.
- (16) Jiang, D.; Su, L.; Ma, L.; Yao, N.; Xu, X.; Tang, H.; Li, X. Cu–Zn–Al mixed metal oxides derived from hydroxycarbonate precursors for H₂S removal at low temperature. *Appl. Surf. Sci.* **2010**, 256, 3216–3223.
- (17) Ryu, S. O.; Park, N. K.; Chang, C. H.; Kim, J. C.; Lee, T. J. Multicyclic study on improved Zn/Ti-based desulfurization sorbents in mid-temperature conditions. *Ind. Eng. Chem. Res.* **2004**, *43*, 1466–1471.
- (18) Flytzani-Stephanopoulos, M.; Sakbodin, M.; Wang, Z. Regenerative adsorption and removal of H₂S from hot fuel gas streams by rare earth oxides. *Science* **2006**, *312*, 1508–1510.
- (19) Li, Z.; Flytzani-Stephanopoulos, M. Cu-Cr-O and Cu-Ce-O regenerable oxide sorbents for hot gas desulfurization. *Ind. Eng. Chem. Res.* **1997**, *36*, 187–196.
- (20) Lew, S.; Sarofim, A. F.; Flytzani-Stephanopoulos, M. Sulfidation of zinc titanate and zinc oxide solids. *Ind. Eng. Chem. Res.* **1992**, *31*, 1890–1899.
- (21) Feng, W.; Kwon, S.; Borguet, E.; Vidic, R. Adsorption of hydrogen sulfide onto activated carbon fibers: effect of pore structure and surface chemistry. *Environ. Sci. Technol.* **2005**, *39*, 9744–9749.
- (22) Adib, F.; Bagreev, A.; Bandosz, T. J. Effect of surface characteristics of wood-based activated carbons on adsorption of hydrogen sulfide. *J. Colloid Interface Sci.* **1999**, 214, 407–415.
- (23) Bagreev, A.; Angel Menendez, J.; Dukhno, I.; Tarasenko, Y.; Bandosz, T. J. Bituminous coal-based activated carbons modified with nitrogen as adsorbents of hydrogen sulfide. *Carbon* **2004**, *42*, 469–476.
- (24) de Oliveira, L. H.; Meneguin, J. G.; Pereira, M. V.; da Silva, E. A.; Grava, W. M.; do Nascimento, J. F.; Arroyo, P. A. H₂S adsorption on NaY zeolite. *Microporous Mesoporous Mater.* **2019**, 284, 247–257. (25) Wynnyk, K. G.; Hojjati, B.; Pirzadeh, P.; Marriott, R. A. High-
- pressure sour gas adsorption on zeolite 4A. Adsorption 2017, 23, 149–162.
- (26) First, E. L.; Hasan, M. M. F.; Floudas, C. A. Discovery of novel zeolites for natural gas purification through combined material screening and process optimization. *AIChE J.* **2014**, *60*, 1767–1785.
- (27) Smith, G. L.; Eyley, J. E.; Han, X.; Zhang, X.; Li, J.; Jacques, N. M.; Godfrey, H. G. W.; Argent, S. P.; McCormick McPherson, L. J.; Teat, S. J.; Cheng, Y.; Frogley, M. D.; Cinque, G.; Day, S. J.; Tang, C. C.; Easun, T. L.; Rudic, S.; Ramirez-Cuesta, A. J.; Yang, S.; Schroder, M. Reversible coordinative binding and separation of sulfur dioxide in a robust metal-organic framework with open copper sites. *Nat. Mater.* **2019**, *18*, 1358–1365.
- (28) Alivand, M. S.; Shafiei-Alavijeh, M.; Tehrani, N. H. M. H.; Ghasemy, E.; Rashidi, A.; Fakhraie, S. Facile and high-yield synthesis of improved MIL-101(Cr) metal-organic framework with exceptional CO₂ and H₂S uptake; the impact of excess ligand-cluster. *Microporous Mesoporous Mater.* **2019**, 279, 153–164.
- (29) Zhao, W.; Veerappan Vaithilingam, B.; Ghosh, S.; Li, X.; Geuzebroek, F.; El Nasr, A. S.; Khan, I.; Dara, S.; Mittal, N.; Daoutidis, P.; Al Hashimi, S.; Mkhoyan, K. A.; Al Wahedi, Y.; Tsapatsis, M.; Stein, A. High-capacity regenerable H₂S sorbent for reducing sulfur emissions. *Ind. Eng. Chem. Res.* **2021**, *60*, 14779—14787.
- (30) Standard test method for single pellet crush strength of formed catalysts and catalyst carriers; ASTM D4179-11(2017); ASTM International: West Conshohocken, PA, 2017. www.astm.org.
- (31) Hoffman, A. S.; Azzam, S.; Zhang, K.; Xu, Y.; Liu, Y.; Bare, S. R.; Simonetti, D. A. Direct observation of the kinetics of gas—solid reactions using in situ kinetic and spectroscopic techniques. *React. Chem. Eng.* **2018**, *3*, 668–675.

- (32) Khalafalla, S. E.; Shah, I. D. Oxidative roasting of covellite with minimal retardation from the CuO·CuSO₄ film. *Metall. Trans. A* **1970**, *1*, 2151–2156.
- (33) Dunn, J. G.; Muzenda, C. Thermal oxidation of covellite (CuS). *Thermochim. Acta* **2001**, 369, 117–123.